JCI insight

# In vivo–directed evolution of adeno-associated virus in the primate retina

Leah C. Byrne, … , David V. Schaffer, John G. Flannery

*JCI Insight.* 2020;5(10):e135112. https://doi.org/10.1172/jci.insight.135112.

Research Article Ophthalmology

## Graphical abstract

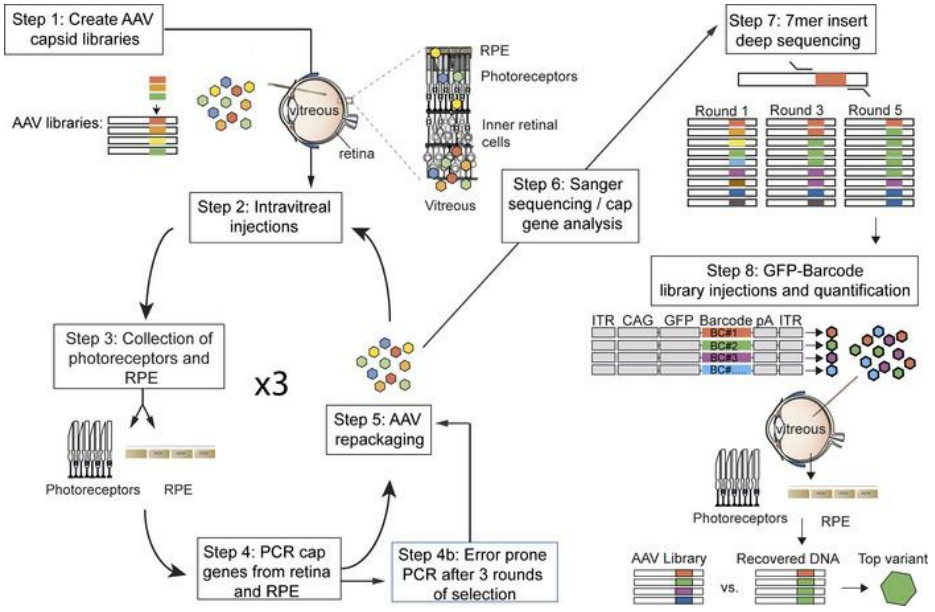


## Find the latest version:

https://jci.me/135112/pdf

JCI insight

RESEARCH ARTICLE

# In vivo–directed evolution of adeno-associated virus in the primate retina

**Leah C. Byrne,[1] Timothy P. Day,[1] Meike Visel,[1] Jennifer A. Strazzeri,[2] Cécile Fortuny,[1] Deniz Dalkara,[3] William H. Merigan,[2] David V. Schaffer,[1] and John G. Flannery[1]**

[1]Helen Wills Neuroscience Institute, University of California, Berkeley, Berkeley, California, USA. [2]Center for Visual Science, David and Ilene Flaum Eye Institute, University of Rochester Medical Center, Rochester, New York, USA. [3]INSERM U968, Institut de la Vision, Paris, France; UMRS968, Institut de la Vision, Sorbonne Universités, Pierre et Marie Curie University/ University Paris 6, Centre National de la Recherche Scientifique UMR7210, Paris, France.

**Efficient adeno-associated virus–mediated (AAV-mediated) gene delivery remains a significant obstacle to effective retinal gene therapies. Here, we apply directed evolution — guided by deep sequencing and followed by direct in vivo secondary selection of high-performing vectors with a GFP-barcoded library — to create AAV viral capsids with the capability to deliver genes to the outer retina in primates. A replication-incompetent library, produced via providing *rep* in *trans*, was created to mitigate risk of AAV propagation. Six rounds of in vivo selection with this library in primates — involving intravitreal library administration, recovery of genomes from outer retina, and extensive next-generation sequencing of each round — resulted in vectors with redirected tropism to the outer retina and increased gene delivery efficiency to retinal cells. These viral vectors expand the toolbox of vectors available for primate retina, and they may enable less invasive delivery of therapeutic genes to patients, potentially offering retina-wide infection at a similar dosage to vectors currently in clinical use.**

**Authorship note:** DVS and JGF contributed equally to this work.

**Conflict of interest:** DVS, LCB, TPD, and JGF are inventors on a patent application for adeno-associated virus (AAV) capsid variants (AAV virions with variant capsid and methods of use thereof) (PCT/US2018/040115, WO/2019/006182). LCB, MV, DVS,and JGF are inventors on a patent application for AAV capsid variants (AAV virions with variant capsid and methods of use thereof) (US8663624B2, EP2699270B1 [7m8 patent]). DD is a paid consultant for GenSight Biologics. DVS is a cofounder of 4D Molecular Therapeutics. LCB was a paid consultant for 4D Molecular Therapeutics.



**Submitted:** November 19, 2019
**Accepted:** April 1, 2020
**Published:** May 21, 2020.

**Reference information:** *JCI Insight*. 2020;5(9):e135112. https://doi.org/10.1172/jci.insight.135112.

## Introduction

Inherited retinal degenerations (RDs) are caused by mutations in more than 200 genes (1), the majority of which are expressed in photoreceptors or retinal pigment epithelium (RPE) of the outer retina, leading to vision loss and decreased quality of life (2, 3). Gene therapy is a promising approach to treating RDs, as evidenced by the recent FDA approval of a gene therapy to treat inherited RDs with biallelic RPE65 mutations. Although the administration of a therapy to the vitreous fluid of the eye offers a simple and less invasive route, compared with the subretinal surgery used for RPE65 and other treatments, as well as the potential to transduce the entire retina, efficient gene delivery to the outer retina in general remains a significant hurdle (4–6). Directed evolution has enabled the creation of new, efficient viral vectors for outer retinal gene delivery in mice (7–9). However, the anatomical features and structural barriers of large-animal retinas are substantially different from mouse (10); for example, large animals have a specialized area for high-acuity vision (the area centralis in dogs or fovea in primates), a vitreous of thicker consistency, and a thicker inner limiting membrane (11, 12). As a result, vectors that were selected for delivery in mouse retina are not as efficient in large-animal models as in rodents (7).

Here, we used directed evolution (13), guided by insights into the population dynamics of viral selections that were derived from deep sequencing, to create adeno-associated viruses (AAVs) capable of delivering genes to outer retina after intravitreal injection in cynomolgus macaques, which have eye structures similar to humans. Subsequently, secondary screening of subsets of the resulting viral variants revealed the most efficient AAVs for photoreceptors and RPE of the primate retina. The outer retinal gene delivery offered by these variants may enable less invasive delivery of therapeutic genes to the retina and potentially provide more expansive transduction at a similar dosage as that currently used in clinical trials.

## Results

*Directed evolution of AAV in primate retina*. The nonhuman primate is a critical preclinical model for human therapeutic development because it has a retinal anatomy similar to that of humans. In particular, the primate is the only large-animal model that possesses a fovea, the specialized high-acuity area of the retina.

The fovea is essential for daily activities such as reading, is critical to quality of life, and is lost in numerous RDs. Here, we have conducted a directed evolution study of AAV in a primate model. Our previous efforts in mouse were based on replication-competent AAV genome libraries; however, primates are known to often harbor a coinfection of herpes B (a helper virus f or AAV). To mitigate the possibility of replication of the AAV libraries in the primate retina and subsequent spread, a *rep* in *trans* strategy was developed in which the library *rep* sequence is mutated (pRepSafeStop) while leaving intact regulatory elements, including the P40 promoter, which is necessary for *cap* protein expression. Stop codons in the *rep* sequence prevented the expression of the 4 Rep proteins, and the full *rep* sequence was supplied on pRepIntronHelper. This system resulted in a greater than 10-fold reduction in replication in the presence of high titers of adenovirus. The inverted terminal repeats (ITRs) in AAV are highly recombinogenic, leading to the possibility of recombination and subsequent replication in the presence of a helper virus when using this strategy, so an intron was inserted in the *rep* supplied in *trans* to prevent packaging of recombined genomes (Figure 1). Replication-incompetent libraries were constructed, packaged, and included in the primate screen, including AAV2-7-mer, Ancestral-7-mer (14), and LoopSwap (15) libraries.

Libraries were injected, harvested, and repackaged for up to 5 sequential rounds of selection, with 1 round of error-prone PCR performed after round 3 (Figure 2 and Supplemental Table 1; supplemental material available online with this article; https://doi.org/10.1172/jci.insight.135112DS1). AAV *cap* genes were PCR amplified from the outer nuclear layer (ONL), which was isolated from transverse cryosections of retina, and in parallel from separated RPE (Supplemental Figure 1).

Deep sequencing (source data 1) revealed that libraries contained approximately $1 \times 10^6$ to $1 \times 10^7$ individual variants, which converged to approximately $1 \times 10^4$ to $1 \times 10^5$ variants over 6 rounds of selection, a diversity not possible to observe through Sanger sequencing (Figure 3A). In each of the libraries analyzed, a small portion of library members were originally overrepresented in the initial plasmid library (Figure 3B). However, relative to this input, analysis of results from deep sequencing over the rounds of selection revealed a subset of variants that increased significantly in their representation during rounds of selection for each of the input libraries (Figure 3C).

*Secondary GFP-barcoded library screening in primate retina*. Twelve variants from the three successfully amplified libraries were chosen for a secondary round of selection with GFP-barcoded libraries, along with parental serotypes as controls. Specifically, each capsid was used individually to package a recombinant genome containing GFP plus a 3′ barcode unique to that capsid. The vectors were diluted until the titers of all variants were equal, as confirmed by quantitative real-time PCR (qRT-PCR), and then the resulting vectors were combined at equal ratios by adding equal volumes of each virus to a pool. This new library was injected in both eyes of a primate, and 3 weeks after injection, biopsies were collected from locations across the retina (Figure 4A). GFP expression resulting from injection of the GFP-barcoded libraries was found in photoreceptors as well as some inner retinal cells (Figure 4B). The ONL and RPE were anatomically isolated, DNA was purified from these samples, and deep sequencing was performed to quantify the relative extents to which each capsid was capable of delivering its genome deep into the retina from the vitreous.

*Validation of the top-performing primate variants*. Quantification of vector performance in the ONL revealed that AAV2-7-mer and LoopSwap–based variants outperformed other viruses (Table 1). The top-ranking vector, LoopSwap variant AAV2 583~LQRGVRIPSVLEVNGQ, outperformed other variants in the GFP-barcoded screen, though it yielded lower viral titers (~$5 \times 10^{11}$ vg/mL). AAV2-LALIQDSMRA (designated NHP#9), the second ranking variant from the GFP-barcoded screen in RPE, was packaged at high titers (~$5 \times 10^{13}$ vg/mL) and therefore selected for a first round of validation studies focusing on ganglion cells of the inner retina and cones of the outer retina. Cone photoreceptors are involved in age-related macular degeneration, the most common cause of blindness in developed countries, and is expected to affect 288 million people worldwide by the year 2040 (16); therefore, cone photoreceptors are a primary target for retinal gene therapy. Retinal ganglion cells (RGCs) are a target for optogenetic and glaucoma therapies (17, 18) and were also targeted for evaluation of inner retinal versus outer retinal transduction.

NHP#9 and the previously described murine variant 7m8 (7) were packaged with a gamma-synuclein gene (SNCG) promoter to drive tdTomato expression in RGCs (19) and the pR1.7 (20) promoter to yield GFP expression in cones. Vectors encoding both these constructs were mixed in equal ratios (~$1.5 \times 10^{12}$ vg/construct/eye) and injected intravitreally in a cynomolgus monkey. The animals were treated with daily subcutaneous injections of cyclosporine (6 mg/kg) for immune suppression, beginning 1 week before AAV injection, and adjusted based on blood trough levels to within a 150–200 ng/ml target range. Expression of tdTomato in RGCs

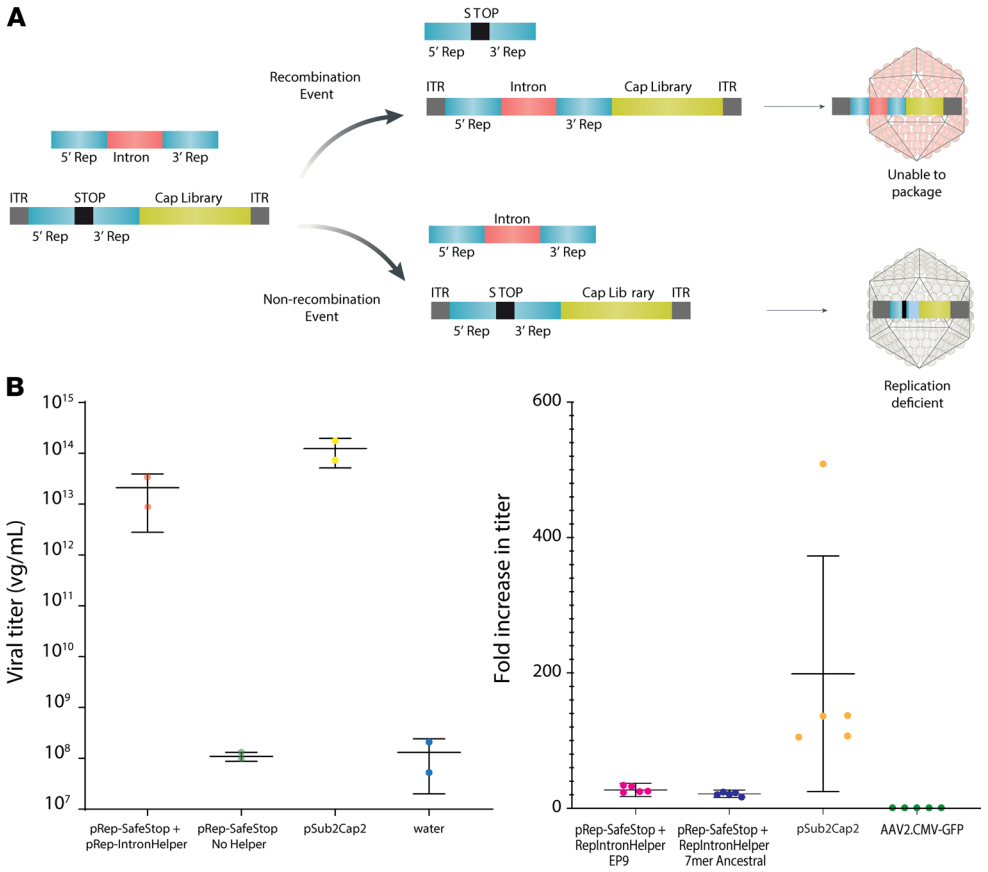


**Figure 1. Replication-incompetent AAV libraries.** (**A**) Schematic depicting both recombination and nonrecombination events with the pRepIntronHelper. If a recombination event were to occur, the intron sequence (*nebulin* intron 8, 774 bp) would push the transgene over the packaging capacity of AAV, leading to incomplete packaging. If recombination does not occur, the mutated *rep* sequence will be packaged, mitigating the possibility of replication. (**B**) Titering of the *rep* in *trans* system with and without pRepIntronHelper, compared with the transgene with native *rep*, pSub2Cap2. The *rep* in trans system leads to similar titers as normal pSub2Cap2 packaging. An adenovirus rescue study determined that the *rep* in trans system leads to a greater than 10-fold reduction in replication. The abilities of an AAV9 error-prone library and the 7-mer-Ancestral library to replicate with the *rep* in *trans* system are shown, compared with an AAV2 with the wild-type genome and a replication-incompetent AAV2 with a CMV-GFP transgene. AAV, adeno-associated virus.

was lower in NHP#9-injected eyes compared with 7m8, which infected ganglion cells across the expanse of the retina efficiently (Figure 5); however, expression in foveal cones was increased relative to 7m8, indicating a shift in tropism away from the inner retina toward photoreceptors in the outer retina. Changes in the efficiency of expression after injection of 7m8 and NHP#9 were evaluated by two methods: the numbers of RGCs and cones infected were quantified by imaging, and qRT-PCR was used to quantify levels of expression in these cells. Quantification of cell numbers, performed using Imaris software on confocal images from the macula, revealed that 7m8 infected 10,310 RGCs, whereas NHP#9 infected 4,296. In contrast, NHP#9 infected 2202 cones, compared with 1019 cones infected by 7m8 (Figure 5, G and H). qRT-PCR, performed using the ΔΔCT method, revealed an 11.71-fold (10.37 to 13.22) increase of GFP expression in foveal cones relative to 7m8.

The top-ranking variant from the GFP-barcoded screen, LoopSwap variant ~583-LQRGVRIPSV-LEVNGQ (designated NHP#26), was also tested for validation despite the limitation that reduced production of this vector enabled only a low dose. Approximately $5 \times 10^{10}$ particles of NHP#26-scCAG-eGFP were injected intravitreally into 1 eye of a cynomolgus monkey. Although the number of particles injected was 30-fold lower than for the other tested vectors, efficient expression of GFP was observed in the fovea and in regions across the retina (Figure 6). In contrast to the foveal-spot-and-ring pattern of expression that was observed with 7m8, NHP#9, and other naturally occurring serotypes, imaging within the foveal region of NHP#26 resulted in a disc of GFP expression centered on the foveola (Figure 6A). Confocal imaging of the flat-mounted retina confirmed this disc pattern of expression around the fovea (Figure 6B), with very few $GFP^+$ ganglion cell axons. Punctate regions of GFP expression were often strongest around retinal blood vessels (Figure 6C) and

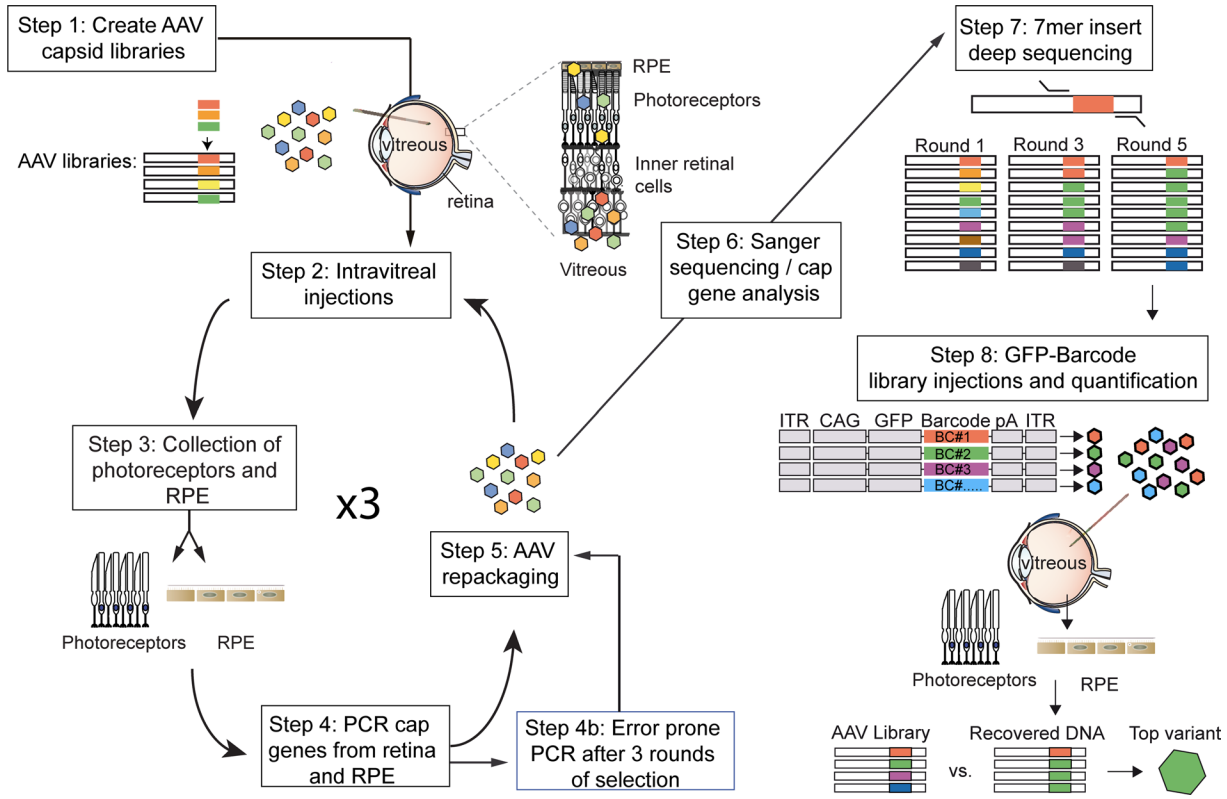


**Figure 2. Workflow of directed evolution of AAV in the primate retina.** Highly diverse (~1 × $10^7$) libraries of AAV variants were packaged such that each virus contained a genome encoding its own capsid. Libraries were pooled and injected intravitreally in primates. After AAV infection had occurred, retinal tissue and RPE cells were collected, and *cap* gene variants were PCR amplified, recloned, and repackaged for the subsequent round of injection. Five rounds of selection were performed, and error-prone PCR was performed after the third round to introduce additional diversity into the library. After the selections, each pool was subjected to deep sequencing to analyze the dynamics of each individual variant and overall convergence of the library. Based on their increase in representation relative to the original library, individual variant capsids were chosen and used to package a scCAG-eGFP genome also containing a unique DNA barcode sequence. These barcoded vectors were then pooled in equal amounts and injected intravitreally. Retinal cells (photoreceptors or RPE cells) were harvested, GFP barcodes were PCR amplified from the collected tissue, and deep sequencing was used to quantify the relative abundance of barcodes. The top-performing variants were evident because those with the greatest fold increase of barcodes recovered from collected tissue relative to the injected library. AAV, adeno-associated virus; RPE, retinal pigment epithelium.

were located across the expanse of the retina. Imaging of cryostat sections taken from the retina confirmed that there was little GFP expression in ganglion cells, as indicated by the lack of $GFP^+$ ganglion cell axons, whereas high levels of GFP expression were found in Müller cells, additional unidentified cells that appeared to have cell bodies in the inner nuclear layer, some foveal cones, and rods across the retina (Figure 6, D–K).

## Discussion

Clinical trials using subretinal surgeries have shown the promise of AAV-mediated gene therapy for retinal disease (21, 22); however, efficient delivery of therapeutic genes across the outer retina — such as from an intravitreal injection — may substantially enhance the safety and retinal area of treatment of gene therapies in such patients. Together, the results described here show that directed evolution, guided by deep sequencing, enabled identification of AAV viruses that were not observable by Sanger sequencing and had an enhanced ability to infect cells in the outer retina of primates, an important preclinical large-animal model for the development of retinal therapies.

Deep sequencing to gain insights into selection dynamics revealed that the variants with the greatest fold increase during selection, rather than the most frequent final variant, is the optimal metric for identifying top-performing variants. Overrepresentation of variants in the original library significantly influenced the number of clones in the final round of selection, with variants that were highly represented in the original library more likely to constitute a majority of clones in the final round and mask more promising variants that were less abundant at the start but that had a greater fold increase over rounds of selection.

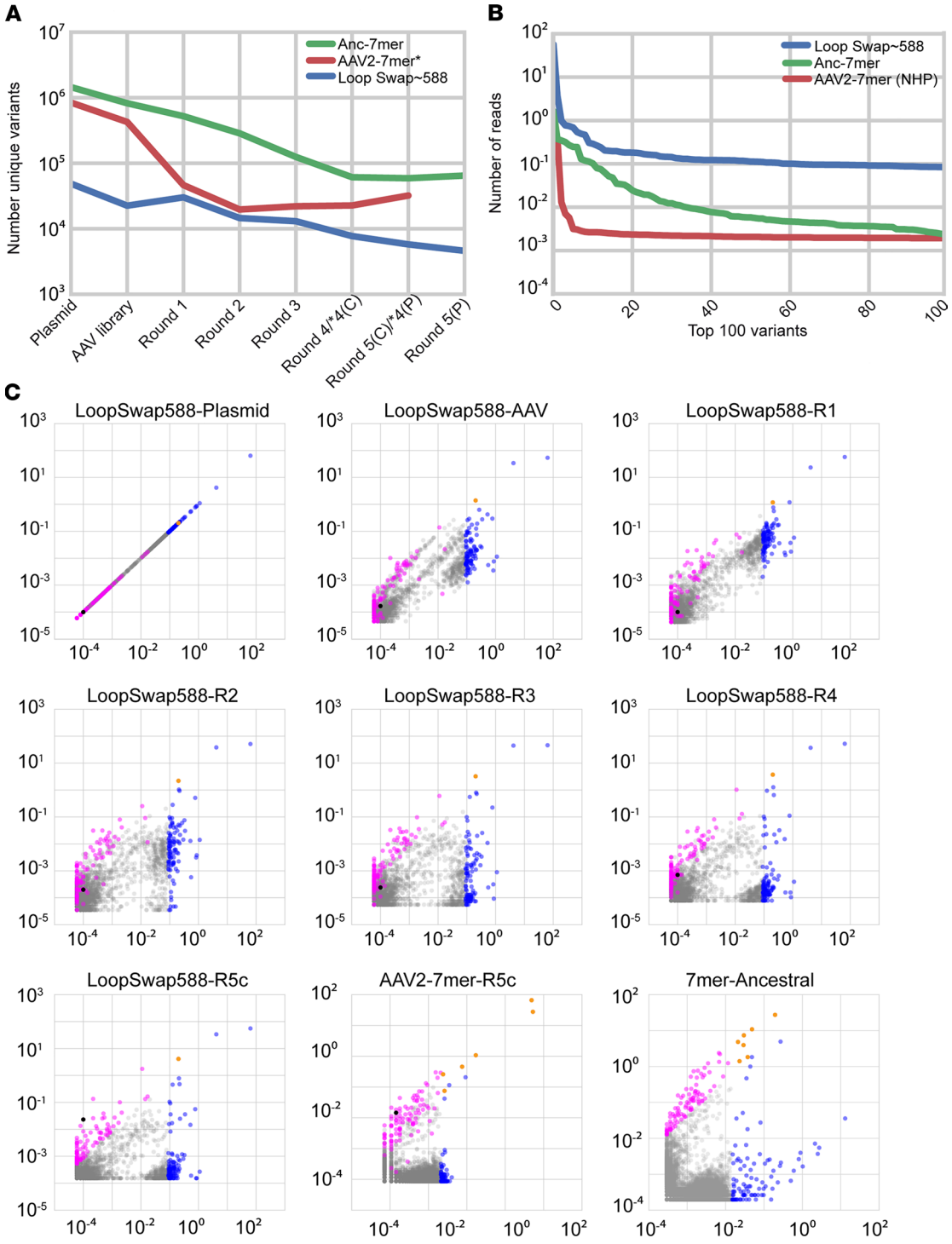


**Figure 3. Directed evolution of AAV in primate retina.** (**A**) Deep sequencing of libraries revealed convergence of variants over rounds of selection. C, central; P, peripheral. (**B**) In each of the libraries evaluated, a small proportion of variants were overrepresented in the plasmid library. (**C**) Scatterplots illustrate the behavior of individual variants over all rounds of selection for the ~588 LoopSwap library for all rounds of selection and at the final round of selection for AAV2-7-mer and 7-mer-Ancestral libraries. Additional scatter plots are shown in Supplemental Figure 2. Black dots in the LoopSwap plots indicate variant NHP#26, validated in Figure 6. The black dot in the AAV2-7-mer plot indicates variant NHP#9, validated in Figure 5. A pseudocount of 1 was added to each variant prior to plotting. *x* axis is the percent of the library made up by each variant in the original library and *y* axis is the percent of total library at the indicated round of selection. As variants increase in representation, they rise on the *y* axis. Variants overrepresented in the original library are colored blue. Variants that had the greatest fold increase in representation in the final round of selection are shown in magenta. Variants that were overrepresented in the original library and increased significantly in representation over rounds of selection are colored orange. From the last round of selection, sequencing was performed on samples from central (R5C, Supplemental Figure 2) and peripheral (R5P) samples separately. AAV, adeno-associated virus.

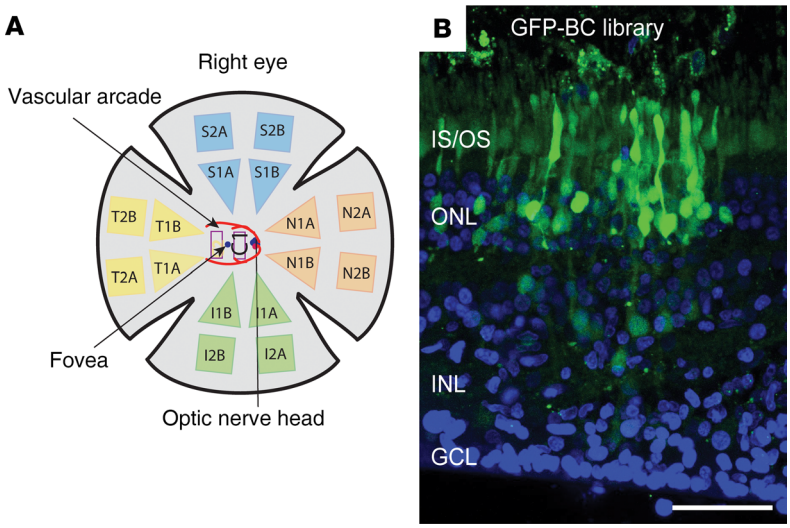


**Figure 4. Directed evolution of AAV in primate retina.** (**A**) A map of the primate retina shows the distribution of samples that were collected for rounds of selection and the GFP-barcoded library. (**B**) GFP expression (shown here from retina along the superior vascular arcade) resulting from the barcoded library revealed that expression was shifted to an outer retinal tropism in selected variants**.** Scale bar: 50 μm. AAV, adeno-associated virus; ONL, outer nuclear layer; INL, inner nuclear layer; GCL, ganglion cell layer.

In addition, the use of GFP-barcoded libraries enabled the selection of AAV variants, from a pool of top-performing candidates identified from deep sequencing, with the best transduction efficiency for the targeted cells. Barcoded-library screening represents a sensitive method for evaluating many variants in parallel, in the same animal, allowing for direct, head-to-head comparison, thus reducing animal numbers (23). Development of vectors in preclinical models must continue to take into account the anatomical differences that exist between species and the possibility that optimization of a therapy in small animals may not translate into large animals with anatomies more similar to humans (24).

AAV variant NHP#9 produced a 2-fold increase in the number of foveal cones infected and an approximately 12-fold increase of GFP expression in foveal cones relative to 7m8. A greater increase in transgene expression relative to the increase in number of cells transfected may be a result of greater numbers of viral particles infecting each cell and/or a greater number of viral particles successfully trafficked to the nucleus. Further experiments are ongoing to discriminate between these possibilities. The variant NHP#26 transduced the outer retina at a titer of $5 \times 10^{10}$ vg, 2 log units lower than the dosage used in a previous study to inject a primate with 7m8 (7). Increasingly, it is understood that an immune response to AAV vectors reduces the transduction efficiency and influences the success of retinal and other gene therapies (25, 26). This vector may enable safer gene therapies for RD in patients as a result of the decreased vector load required for transgene expression and may reduce risk of vector-related toxicity or immunogenicity. Here, we used daily dosage of an immune suppressant in primates injected with GFP-encoding vectors. Temporary immune suppression is commonly used in clinical trials of ocular gene therapies, but long-term or permanent immune suppression is likely not feasible. Further work is required to determine an optimal regimen and the period during which immune suppression may be required, or if immune suppression may be tapered off after an initial critical period.

Additional studies into the composition of physical barriers, including the vitreous and inner limiting membrane, may elucidate the physical basis for the patterns of expression seen after intravitreal injection. Furthermore, directed evolution screens isolating variants from specific retinal locations, such as the macula, may result in variants with increased capabilities to target these areas, because results from the present screens represent an average across the retina. Deeper characterization of the vectors created in this study will likely lead to additional mechanistic insights into cell targeting and tropism.

## Methods

*Construction of the pRepSafeStop directed evolution backbone*. The pRepSafeStop plasmid containing a *Not* I site for *cap* cloning was created by Quikchange site-directed mutagenesis (SDM) on pSub2Cap2 to introduce

**Table 1. Rankings of variants after injection of GFP-barcoded library**

| ONL | | | RPE | | |
|---|---|---|---|---|---|
| **Insert sequence** | **Source library** | **Value** | **Insert sequence** | **Source library** | **Value** |
| LQRGVRIPSVLEVNGQ | LS588 central | 61.2 | LQRGVRIPSVLEVNGQ | LS588 Central | 33.66 |
| LQKADRQPGVVVVNCQ | LS588 peripheral | 2.75 | LALIQDSMRA | AAV2-7-mer central | 4.63 |
| LQKNARPASTESVNFQ | LS588 central | 2.75 | LTHQDTTKNA | AAV2-7-mer central | 4.12 |
| AAV24YF+ | Control | 1.69 | QAHQDTTKNA | AAV2-7-mer peripheral | 3.42 |
| AAV2 | Control | 1.61 | LANQEHVKNA | AAV2-7-mer peripheral | 2.25 |
| LQRGNRPVTTADVNTQ | LS588 peripheral | 1.29 | NGAVADYTRGLSPATGT | Anc-7-mer peripheral | 1.55 |
| QAHQDTTKNA | AAV2-7-mer peripheral | 0.77 | TGLDATRDHGLSPVTGT | Anc-7-mer central | 1.04 |
| TGLDATRDHGLSPVTGT | Anc-7-mer central | 0.71 | LQKADRQPGVVVVNCQ | LS588 peripheral | 0.98 |
| NGAVADYTRGLSPATGT | Anc-7-mer peripheral | 0.52 | LQRGNRPVTTADVNTQ | LS588 peripheral | 0.69 |
| TGGDPTRGTGLSPVTGA | Anc-7-mer peripheral | 0.37 | AAV24YF+ | Control | 0.57 |
| TGSDGTRDHGLSPVTWT | Anc-7-mer central | 0.28 | AAV2 | Control | 0.56 |
| LALIQDSMRA | AAV2-7-mer central | 0.22 | LQKNARPASTESVNFQ | LS588 central | 0.52 |
| LANQEHVKNA | AAV2-7-mer peripheral | 0.20 | TGGDPTRGTGLSPVTGA | Anc-7-mer peripheral | 0.48 |
| LTHQDTTKNA | AAV2-7-mer central | 0.20 | TGSDGTRDHGLSPVTWT | Anc-7-mer central | 0.47 |

The lists of variants are ordered from best- (top) to worst-performing (bottom) vectors, along with a description of the source library and the sample the variant was identified from (central or peripheral) and a value indicating the extent to which the variant competed with other vectors, expressed as: percentage of total in recovered library/percentage of total in AAV library. ONL, outer nuclear layer; RPE, retinal pigment epithelium.

stop codons in *rep* at codons 5 and 235 using pRepSafeStop SDM primers. Unique pRepSafeStop backbones containing *Asc* I and *Spe* I sites were created via Gibson Assembly to maintain separation of libraries through rounds of selection. Libraries were PCR amplified and digested with *Hind* III and *Not* I/*Asc* I/*Spe* I and then ligated into the pRepSafeStop construct.

*Rep intron helper cloning*. Intron 8 from the *nebulin* gene was amplified from genomic DNA isolated from HEK293T cells using the Neb Genomic primers and cloned into a TOPO vector. To create the pRepIntron-Helper, the rh10 AAV helper plasmid pAAV2/rh10 was digested with *Pme* I and *Bsm* I, Klenow blunting was performed, and the resulting DNA fragment was recircularized. The first AGG sequence after the Rep52/Rep40 start codon was chosen as the site for intron insertion based on a computational analysis of splice signal motifs. Infusion assembly (IFA) was used to insert the *nebulin* intron using the IFA primers, thereby generating the final plasmid.

*Adenovirus rescue to determine loss of AAV replication with the pRepSafeStop backbone*. HEK293T cells were infected with AAV (AAV2, an EP9 variant and a 7-mer Ancestral variant) at a MOI of $10^5$ and then incubated at 37°C and 5% $CO_2$ for 48 hours. Next, 10 μL of an adenovirus 5 (Ad5) stock, a volume that resulted in cytopathic effect within 24 hours, was added and the plates were incubated at 37°C and 5% $CO_2$ for an additional 48 hours. Cells that were then harvested, pelleted, and resuspended in 100 μL lysis buffer (0.15 M NaCl, 50 mM Tris HCl, 0.05% Tween, pH 8.5). Freeze/thaws cycles were used to lyse the cells, and 5 μL of the crude lysate was used for titering AAV to quantify replication.

*AAV selection in primate outer retina*. Three weeks after intravitreal injection, the primate was euthanized, and both eyes, as whole globes, were briefly submerged in 4% paraformaldehyde. Superior, inferior, temporal, and nasal regions of the retina were cut into 4 equal pieces, and the RPE was separated from each section. Retinal sections were then immersed in 30% sucrose, embedded in OCT media, and flash frozen. Retinal pieces were sectioned transversely at 20 μm. During sectioning, DAPI staining and light microscopy were used to identify each nuclear layer in the retina, and the inner nuclear and ganglion cell layers were removed. DNA was extracted from samples using a QIAGEN DNeasy blood and tissue kit, according to manufacturer's instructions.

*AAV packaging*. AAV libraries were constructed prior to this study and have been previously described (7, 13, 27, 28). After each round of injection, capsid sequences were recovered by PCR from harvested cells using primers HindIII_F1 and NotI_R1, AscI_R1, or SpeI_R1, with reverse primers being specific to unique AAV backbones, to maintain separation of groups of libraries. PCR amplicons were then digested and recloned into the AAV pRepSafeStop backbone. AAV packaging has been described previously (29). AAV vectors with pRepSafeStop backbone were produced by triple transient

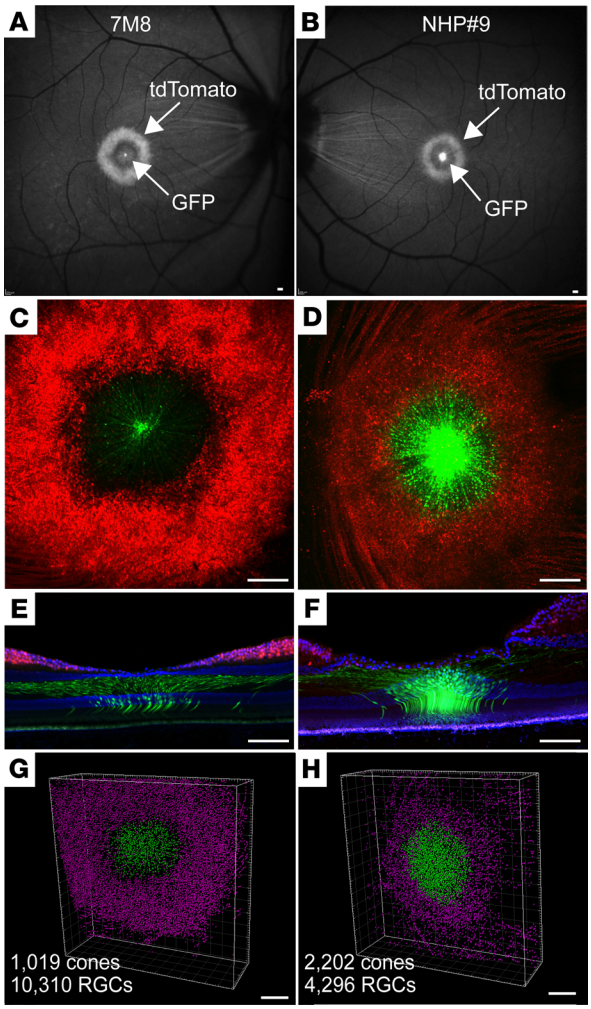


**Figure 5. Validation of NHP#9 in primate retina.** Coinjection of approximately $1.5 \times 10^{12}$ particles of SNCG-tdTomato and approximately $1.5 \times 10^{12}$ pR1.7-eGFP packaged in 7m8 and variant NHP#9 in primate retina. Intravitreal injection of 7m8 (**A**, **C**, and **E**) resulted in robust tdTomato expression in ganglion cells and expression of GFP in foveal cones. In contrast, injection of equal number of particles of NHP#9 in the contralateral eye resulted in reduced ganglion cell expression and increased GFP expression in cones relative to 7m8 (**B**, **D**, and **F**). (**G** and **H**) Quantification of ganglion cells and cones transduced with 7m8 and NHP#9 in primate retina. Counting of labeled cells, performed using Imaris software, revealed a substantial decrease in the numbers of transduced ganglion cells and an increase in the number of cones targeted with NHP#9, compared with 7m8. Scale bar: 200 μm (**A** and **B**), 100 μm (**C**–**F**), 200 μm (**G** and **H**). SNCG, gamma-synuclein gene.

transfection of HEK293T cells (from ATCC) with the addition of the pRepIntronHelper plasmid in 5 times greater concentration than the library plasmid, purified via iodixanol density centrifugation, and buffer exchanged into PBS by Amicon filtration. DNAse-resistant viral genomic titers were measured by qRT-PCR using a Bio-Rad iCycler.

*Deep sequencing of AAV libraries from rounds of selection*. An approximately 75- to 85-bp region containing the 7-mer insertion or LoopSwap mutation sites (semirandom mutations at surface-exposed regions; see ref. 15 for a description of LoopSwap library construction) was PCR amplified from harvested DNA. Primers included Illumina adapter sequences containing unique barcodes to allow for multiplexing of amplicons from multiple rounds of selection (Supplemental Table 2). PCR amplicons were purified and sequenced with a 100-cycle single-read run on an Illumina HiSeq 2500. Custom Python code was written for analysis. First, the DNA sequences encoding amino acid insertions, found between constant linker DNA sequences, were identified. Then DNA sequences were translated into amino acid sequences. The number of reads for each amino acid insertion sequence was then counted, across the AAV library and across rounds of selection. Read counts were normalized by the total number of reads in the run. Pandas was used to analyze dynamics of directed evolution and create plots.

*Deep-sequencing analysis*. Deep sequencing was performed at more than 10× depth of the number unique variants in the round. Reads with low-quality scores were eliminated from further analysis using Illumina workflow. Variants were analyzed on the amino acid level (i.e., variants with varying DNA sequences encoding the same amino acid sequence were pooled together for analysis). Best performing variants were chosen as variants with the greatest fold increase in the final round of selection relative to the initial plasmid library (number reads in final round, normalized to total number of reads in the round/number of reads in library, normalized to total number of reads in the round). A pseudocount of 1 was added before

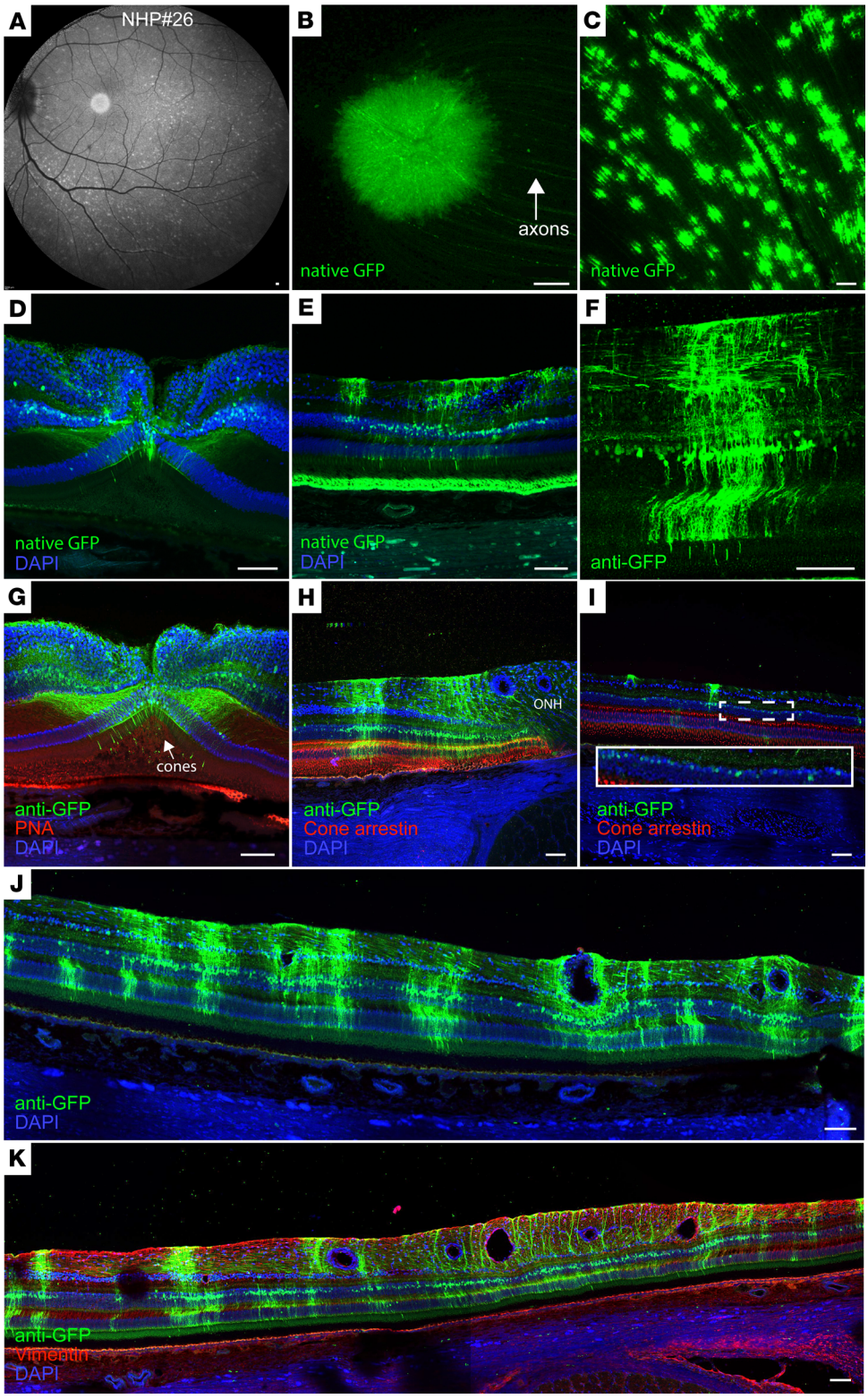


**Figure 6. Validation of NHP#26 in primate retina.** (**A**) Fundus imaging in a primate eye after injection of $5 \times 10^{10}$ particles of NHP#26-scCAG-GFP revealed a disc of GFP expression centered on the fovea and a punctate pattern of GFP expression across the retina. (**B**) Confocal imaging of native GFP expression in the flat-mounted fovea. (**C**) Confocal imaging of native GFP expression in the area outside of the vascular arcade. (**D**) Confocal imaging of native GFP expression in a cryostat section through the fovea. (**E**) Native GFP expression in the inferior retina, outside the vascular arcade, shows little GFP expression in ganglion cells, but shows high levels of expression in Müller cells and some photoreceptors in the outer retina. Autofluorescence was also observed in RPE. (**F**) Anti-GFP labeling in a cryostat section revealed GFP expression in photoreceptors, as evidenced by their outer segments, Müller cells, and retina-spanning processes as well as cells in the inner nuclear layer with horizontal processes that are likely interneurons. (**G**) Anti-GFP labeling in a foveal section reveals additional infected cones, Müller glia, and interneurons. (**H**) Colabeling with anti–cone arrestin and anti-GFP antibodies reveals GFP expression in rod photoreceptors as well as cells in the inner nuclear layer, in a section taken next to the optic nerve head. (**I**) Colabeling with anti–cone arrestin and anti-GFP antibodies in an area of low expression reveals GFP expression in inner nuclear layer cells. (**J** and **K**) Montages of confocal images from cryostat sections collected outside the vascular arcade show efficient expression of GFP in the inner nuclear layer and outer retina. Scale bar: 200 μm (**A** and **B**), 100 μm (**C**–**K**). RPE, retinal pigment epithelium.

normalization to each individual variant to allow analysis of variants not appearing in sequencing of the plasmid library (30).

*GFP-barcoded library construction*. Unique 25-bp DNA barcodes were cloned behind a self-complementary AAV ITR construct containing a CAG promoter driving eGFP (CAG-GFP-Barcode-pA). Individual variants were packaged separately with constructs containing different barcodes. Variants were then titer matched and mixed in equal ratios before injection into primates.

*Deep sequencing of GFP-barcoded libraries*. Barcodes were PCR amplified directly from DNA, which was harvested from primate retinal tissue. Samples were collected from areas across the retina and from ONL or RPE. Primers amplified an approximately 50-bp region surrounding the GFP barcode and contained Illumina adapter sequences and secondary barcodes to allow for multiplexing of multiple samples (Supplemental Table 2). PCR amplicons were purified and sequenced with a 100-cycle single-read run on a MiSeq. Read counts were normalized by total number of reads in the run. Analysis of barcode abundance was performed using custom code written in Python, followed by creation of plots in Pandas. Barcodes were identified as variable DNA sequences found between constant sequences in the expression cassette, which surrounded the barcode. Best performing variants were selected based on the fold increase in the percent of total library, relative to the injected library (percentage of total in recovered sample/percentage of total in injected library). Analysis was performed on $n = 1$ primate.

*Gene expression analysis*. GFP expression was calculated relative to GAPDH, using the ΔΔCT method on RNA collected from retinal sections and extracted using AllPrep DNA/RNA FFPE Kit (QIAGEN). Tests were performed in triplicate with technical replicates from the same eye.

*Primers*. Primer sequences are listed in Supplemental Table 2.

*Animal studies*. C57BL/6 mice from Jackson Laboratories were used for mouse experiments. Surgery was performed under anesthesia, and all efforts were made to minimize suffering.

Cynomolgus monkeys (Valley Biosystems) between 4 and 10 years old were used for all studies, and intravitreal injections were made with methods described previously (6). To prevent any immune response to GFP or viral vectors, which have been previously reported (7), the monkey used for fluorophore expression received daily subcutaneous injections of cyclosporine at a dose of 6 mg/kg for immune suppression, beginning 1 week before AAV injection, and the dosage regimen was adjusted based on blood trough levels to within a 150–200 ng/ml target range. All primates were screened for neutralizing antibodies prior to inclusion in the study and had titers less than 1:25. Confocal scanning laser ophthalmoscopic images (Spectralis HRA, Heidelberg Engineering) were obtained 3 weeks after injection, with autofluorescence settings, which lead to effective tdTomato and GFP visualization. For histology, the monkey was euthanized, both retinas were lightly fixed in 4% paraformaldehyde, and tissue was examined by confocal microscopy. At the conclusion of the experiment, euthanasia was achieved by administering an i.v. overdose of sodium pentobarbital (75 mg kg−1), as recommended by the Panel on Euthanasia of the American Veterinary Medical Association. Pieces of primate retina were then prepared in 30% sucrose, embedded in OCT media, flash frozen, and sectioned at 20 μm for confocal microscopy imaging of native fluorophore expression. Antibodies for labeling were as follows: anti-GFP (A11122, Thermo, 1:250); anti-vimentin (Dako, 1:1000); peanut agglutinin (PNA, Molecular Probes, 1:200); anti-PKC alpha (ab32376, Abca, 1:1000); and anti–cone arrestin (7G6, gift from Peter MacLeish, Morehouse School of Medicine, Atlanta, Georgia, 1:50). A summary of minor adverse events related to the procedures is summarized in Supplemental Table 1.

*Data and materials availability*. Raw counts from deep-sequencing data sets are available on Dash, the University of California data sharing service (31).

*Study approval*. All procedures performed on mice were in accordance with the ARVO statement for the Use of Animals in Ophthalmic and Vision Research and approved by the University of California Animal Care and Use Committee (AUP R200-0913BC). The procedures conducted on primates were in accordance with the ARVO Statement for the Use of Animals and the guidelines and were performed with approval from of the Office of Laboratory Animal Care at the University of Rochester.

## Author contributions

LCB conceived, planned, and executed experiments; analyzed data; and wrote the manuscript. TPD conceived, planned, and executed primate experiments; analyzed data; and wrote the manuscript. MV planned the experiments, performed AAV packaging, analyzed data, and wrote the manuscript. DD performed directed evolution screening in macaque retina, provided AAV constructs with PR1.7/SNCG promoters, and wrote the manuscript. WHM supervised intravitreal injection and fluorescent fundus imaging of viral vectors in macaques and wrote the manuscript. CF conceived, planned, and executed experiments and analyzed data. JAS performed macaques experiments and wrote the manuscript. DVS conceived, planned, and supervised the project and wrote the manuscript. JGF conceived, planned, and supervised the project and wrote the manuscript.

## Acknowledgments

Deep sequencing was performed at the QB3 Vincent J. Coates Genomics Sequencing Laboratory. Confocal imaging was performed at the Berkeley Biological Imaging Facility. Injections for AAV selection in primates were performed at Valley Biosystems. We thank Yvonne Lin, and Jaskiran Mann for technical assistance. Funding was provided by the Ford Foundation, National Eye Institute/NIH (F32EY023891, PN2EY01824), 4D Molecular Therapeutics, and Foundation Fighting Blindness.

Address correspondence to: David V. Schaffer, 278 Stanley Hall, Berkeley, California 94720-3220, USA. Phone: 510.642.4923; Email: schaffer@berkeley.edu. Or to: John G. Flannery, 132 Barker Hall, Berkeley, California 94720-3190, USA. Phone: 510.642.0209; Email: flannery@berkeley.edu.

LCB's present address is: Departments of Ophthalmology, Neurobiology and Bioengineering, University of Pittsburgh, Pittsburgh, Pennsylvania, USA.

DD's present address is: Sorbonne Université, Institut de la Vision, INSERM, CNRS, Paris, France.

1. Daiger SP. RetNet – Retinal Information Network. University of Texas. https://sph.uth.edu/retnet. Accessed April 9, 2020.
2. Wright AF, Chakarova CF, Abd El-Aziz MM, Bhattacharya SS. Photoreceptor degeneration: genetic and mechanistic dissection of a complex trait. *Nat Rev Genet*. 2010;11(4):273–284.
3. Boye SE, Boye SL, Lewin AS, Hauswirth WW. A comprehensive review of retinal gene therapy. *Mol Ther*. 2013;21(3):509–519.
4. Cepko CL. Emerging gene therapies for retinal degenerations. *J Neurosci*. 2012;32(19):6415–6420.
5. Dalkara D, et al. Inner limiting membrane barriers to AAV-mediated retinal transduction from the vitreous. *Mol Ther*. 2009;17(12):2096–2102.
6. Yin L, et al. Intravitreal injection of AAV2 transduces macaque inner retina. *Invest Ophthalmol Vis Sci*. 2011;52(5):2775–2783.
7. Dalkara D, et al. In vivo-directed evolution of a new adeno-associated virus for therapeutic outer retinal gene delivery from the vitreous. *Sci Transl Med*. 2013;5(189):189ra76.
8. Kotterman MA, Schaffer DV. Engineering adeno-associated viruses for clinical gene therapy. *Nat Rev Genet*. 2014;15(7):445–451.
9. Klimczak RR, Koerber JT, Dalkara D, Flannery JG, Schaffer DV. A novel adeno-associated viral variant for efficient and selective intravitreal transduction of rat Müller cells. *PLoS One*. 2009;4(10):e7467.
10. Matsumoto B, Blanks JC, Ryan SJ. Topographic variations in the rabbit and primate internal limiting membrane. *Invest Ophthalmol Vis Sci*. 1984;25(1):71–82.
11. Heegaard S, Jensen OA, Prause JU. Structure and composition of the inner limiting membrane of the retina. SEM on frozen resin-cracked and enzyme-digested retinas of Macaca mulatta. *Graefes Arch Clin Exp Ophthalmol*. 1986;224(4):355–360.
12. Beltran WA, et al. Canine retina has a primate fovea-like bouquet of cone photoreceptors which is affected by inherited macular degenerations. *PLoS One*. 2014;9(3):e90390.
13. Maheshri N, Koerber JT, Kaspar BK, Schaffer DV. Directed evolution of adeno-associated virus yields enhanced gene delivery vectors. *Nat Biotechnol*. 2006;24(2):198–204.
14. Santiago-Ortiz J, et al. AAV ancestral reconstruction library enables selection of broadly infectious viral variants. *Gene Ther*. 2015;22(12):934–946.
15. Koerber JT, Klimczak R, Jang JH, Dalkara D, Flannery JG, Schaffer DV. Molecular evolution of adeno-associated virus for enhanced glial gene delivery. *Mol Ther*. 2009;17(12):2088–2095.
16. Wong WL, et al. Global prevalence of age-related macular degeneration and disease burden projection for 2020 and 2040: a systematic review and meta-analysis. *Lancet Glob Health*. 2014;2(2):e106–e116.
17. Scholl HP, et al. Emerging therapies for inherited retinal degeneration. *Sci Transl Med*. 2016;8(368):368rv6.
18. Berry MH, et al. Restoration of high-sensitivity and adapting vision with a cone opsin. *Nat Commun*. 2019;10(1):1221.
19. Chaffiol A, et al. A new promoter allows optogenetic vision restoration with enhanced sensitivity in macaque retina. *Mol Ther*. 2017;25(11):2546–2560.
20. Ye GJ, et al. Safety and biodistribution evaluation in cynomolgus macaques of rAAV2tYF-PR1.7-hCNGB3, a recombinant AAV vector for treatment of achromatopsia. *Hum Gene Ther Clin Dev*. 2016;27(1):37–48.
21. Jacobson SG, et al. Improvement and decline in vision with gene therapy in childhood blindness. *N Engl J Med*. 2015;372(20):1920–1926.
22. Cideciyan AV, et al. Human retinal gene therapy for Leber congenital amaurosis shows advancing retinal degeneration despite enduring visual improvement. *Proc Natl Acad Sci U S A*. 2013;110(6):E517–E525.
23. Adachi K, Enoki T, Kawano Y, Veraz M, Nakai H. Drawing a high-resolution functional map of adeno-associated virus capsid by massively parallel sequencing. *Nat Commun*. 2014;5:3075.
24. Hordeaux J, Wang Q, Katz N, Buza EL, Bell P, Wilson JM. The Neurotropic Properties of AAV-PHP.B Are Limited to C57BL/6J Mice. *Mol Ther*. 2018;26(3):664–668.
25. Reichel FF, et al. AAV8 can induce innate and adaptive immune response in the primate eye. *Mol Ther*. 2017;25(12):2648–2660.
26. Bainbridge JW, et al. Long-term effect of gene therapy on Leber's congenital amaurosis. *N Engl J Med*. 2015;372(20):1887–1897.
27. Koerber JT, Jang JH, Schaffer DV. DNA shuffling of adeno-associated virus yields functionally diverse viral progeny. *Mol Ther*. 2008;16(10):1703–1709.
28. Koerber JT, Maheshri N, Kaspar BK, Schaffer DV. Construction of diverse adeno-associated viral libraries for directed evolution

of enhanced gene delivery vehicles. *Nat Protoc*. 2006;1(2):701–706.
29. Grieger JC, Choi VW, Samulski RJ. Production and characterization of adeno-associated viral vectors. *Nat Protoc*. 2006;1(3):1412–1428.
30. Fowler DM, Stephany JJ, Fields S. Measuring the activity of protein variants on a large scale using deep mutational scanning. *Nat Protoc*. 2014;9(9):2267–2284.
31. Byrne L, et al. Directed evolution of AAV for efficient gene delivery to canine and primate retina - raw counts of variants from deep sequencing. University of California, Berkeley. https://doi.org/10.6078/D1895R. Accessed April 24, 2020.